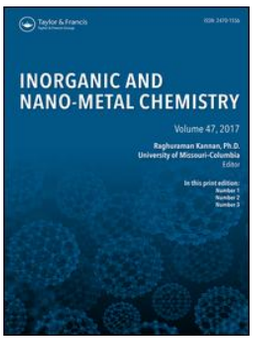

Inorganic and Nano-Metal Chemistry

ISSN: (Print) (Online) Journal homepage: https://www.tandfonline.com/loi/lsrt21

Spectroscopic, DFT analysis, antimicrobial and cytotoxicity studies of three gold(III) complexes

Ramadan M. Ramadan, Amani F. H. Noureldeen, Mohamed M. Abo-Aly & Samir M. El-Medani

To cite this article: Ramadan M. Ramadan, Amani F. H. Noureldeen, Mohamed M. Abo-Aly & Samir M. El-Medani (2021): Spectroscopic, DFT analysis, antimicrobial and cytotoxicity studies of three gold(III) complexes, Inorganic and Nano-Metal Chemistry, DOI: 10.1080/24701556.2021.1891102

To link to this article: https://doi.org/10.1080/24701556.2021.1891102

INORGANIC AND NANO-METAL CHEMISTRY
https://doi.org/10.1080/24701556.2021.1891102

Spectroscopic, DFT analysis, antimicrobial and cytotoxicity studies of three gold(III) complexes

Ramadan M. Ramadan[a], Amani F. H. Noureldeen[b], Mohamed M. Abo-Aly[a], and Samir M. El-Medani[c]

[a]Chemistry Department, Faculty of Science, Ain Shams University, Cairo, Egypt; [b]Department of Biochemistry, Faculty of Science, Ain Shams University, Cairo, Egypt; [c]Chemistry Department, Faculty of Science, Fayoum University, Fayoum, Egypt

ABSTRACT

Three gold(III) complexes were synthesized using 2-pyrazinecarboxamide, pyridine or bipyridine ligand. Complexes were characterized by spectroscopic and analytical techniques (IR, Raman, 1H NMR, mass spectrometry and elemental analysis). Thermogravimetry and conductivity of complexes were investigated. IR, Raman and theoretical calculations of spectral modes of vibrations using DFT and MP2 methods were performed. Biological activities of the complexes against two bacteria *Escherichia coli* and *Staphylococcus aureus* and two fungi *Aspergillus flavus* and *Candida albicans* were screened. They exhibited activities toward both bacteria and fungi. Potency assays of the complexes against two breast cancer and liver carcinoma cell lines were evaluated. They exhibited *in vitro* activities toward the tumors relative to *cis*-platin. In addition, fluorescence quenching studies viscosity measurements of the complexes are performed. Theoretical calculations based on accurate DFT were established to verify the optimized structures of complexes. Global chemical reactivity descriptors were estimated from energy of HOMO and LUMO orbitals.

ARTICLE HISTORY
Received 1 September 2020
Accepted 1 December 2020

KEYWORDS
Pyrazine derivatives; gold complexes; IR and Raman studies; DFT studies; anticancer drugs

1. Introduction

Transition-metal-based complexes represent important class of chemotherapeutics, widely used in the clinical centers as antitumor and antiviral agents. They offer potential advantages over the more common organic-based drugs. Vast efforts are committed to develop novel transition metal-based derivatives, such as platinum, gold and ruthenium complexes. These complexes may have higher antitumor activity and overcome the disadvantages of *cis*-platin (The more established antitumor metallodrug).[1–6] Considerable amount of interest has focused on the use of platinum complexes with pyridine bases as mimics of *cis*-platin.[7,8] These studies have shown that the use of planar ligands, such as the substituted pyridines in platinum (II) complexes, can reduce the rate of deactivation by sulfhydryl groups without interfering with DNA binding, considered to be the mode of action of *cis*-platin.[7–10] On the other hand, Au(III) complexes have shown to be particularly promising class of anticancer agents. The development of various types of ligands capable of stabilizing the Au(III) cation in physiological conditions (nitrogen-donor based, dithiocarbamate and cyclometalled ligands) opened the way for exploration of their mechanisms of action. At the same time, the bio-conjugation of Au(III) complexes has emerged as a potential way for improving the selectivity of this class of compounds for cancer cells over healthy tissues.[5] Gold(III) complexes showed chemical features that are very close to those of clinically employed platinum(II) complexes, such as the preference for square planar coordination and the typical d^8 electronic configuration.[5,11] However, for gold complexes, especially those adapted different structures than square planer, we cannot rule out the interaction of with DNA as one of the possible mechanisms. Recently, there are many reports appeared to explore the use of gold(III) complexes as anticancer drugs.[11–16] Various classes of gold(III) compounds, such as gold(III) dithiocarbamates,[17] gold(III) porphyrinates,[18] dinuclear gold(III) complexes[19] and a variety of organogold(III) compounds,[20] were prepared and characterized showing an appreciable stability under physiological-like conditions and manifesting at the same time important *in vitro* antiproliferative effects. Moreover, for a few gold(III) compounds, preliminary but truly encouraging *in vivo* data were obtained.[13,21]

Our interest in the synthesis of various transition metal complexes with heterocyclic ligands, which they have appropriate biological activities and showed promising applications as antitumor drugs[3,4,8] has prompted us to continue the investigation of some gold complexes of these ligands. In this article, we report the synthesis, characterization and the biological activity (including antimicrobial, cytotoxicity, fluorescence quenching and viscosity measurements) of three Au(III) complexes. Although the characterization of most previously reported complexes involved infrared studies, there are less extensive Raman analyses were observed. In addition, the infrared analysis was generally limited to certain narrow regions. Therefore, we studied the reported gold complexes using infrared, Raman as well as the

CONTACT Ramadan M. Ramadan r_m_ramadan@yahoo.com Chemistry Department, Faculty of Science, Ain Shams University, Cairo, Egypt.
Supplementary data for this material can be accessed at https://doi.org/10.1080/24701556.2021.1891102.

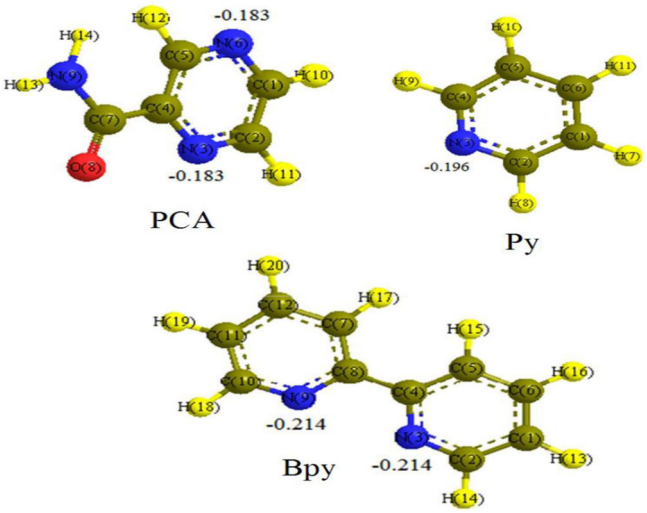

Figure 1. Structure of ligands with the charge density indicated on the donor nitrogen atoms.

theoretical calculations of the spectral modes of vibrations using DFT and MP2 methods. The optimized structures of the complexes were also explored using DFT calculations. Figure 1 gives the structure of the ligands used in the study.

2. Experimental methods

2.1. Materials and instruments

Gold(III) chloride and the heterocyclic nitrogen donor ligands were purchased from Aldrich. All the solvents were of analytical reagent grade and were purified using standard methods. IR measurements were carried out on a Unicam-Mattson 1000 FT-IR (4000–400 cm^{-1}) as KBr pellets. Raman spectra were measured on a dispersive Raman spectrometer of Santerra-Bruker, with a wavelength of 785 nm, laser power of 10 mW and a resolution of 9.18 cm^{-1}. The samples in the solid form were deposited on a slide and the spectrum was recorded using a small value laser power to prevent any photodegradation of the complexes during Raman measurements. ^{1}H and ^{13}C NMR measurements were performed on a Spectrospin-Bruker 300 MHz spectrometer using DMSO, d_6 solvent. Thermogravimetric analysis measurements were carried out (N_2 atmosphere) at a heating rate of 10 °C/min using a Shimadzu DT-50 thermal instrument. Elemental analyses were measured using Perkin-Elmer 2400 CHN elemental analyzer. Mass spectrometry measurements of the solid complexes (70 eV, EI) were carried out on a Finnigan MAT SSQ 7000 spectrometer. Conductivity measurements were made on a YSE conductivity meter model 32. Samples of concentration ca. 1 × 10-3-1 × 10-6 M in DMSO were used for the measurements.

2.2. Synthesis of complexes

2.2.1. Synthesis of AuPCA complex

A solution of **PCA** ligand (0.5 mmol) in a minimum amount of ethanol is added dropwise with constant stirring to a 0.5 mmol aqueous ethanol solution of $AuCl_3$. The mixture was heated for ½ h at 60 °C, at which the complex was precipitated. The resultant residue was filtered off and washed with hot petroleum ether. The obtained residue was recrystallized from hot ethanol. The isolated fine crystals were left to dry under vacuum for 5–6 h.

AuPCA: $C_5H_5N_3OCl_3Au$: Orange red. M.Wt.=426.44. Yield: 58%. Elemental analysis, Found (Calc.): % C = 14.05 (14.08); % H = 1.15 (1.18); % N = 9.80 (9.85); % Cl = 24.98 (24.94). Mass spectrometry (m/z)=391 $[P–Cl]^+$.

2.2.2. Synthesis of AuPy and AuBpy complexes

An equimolar mixture of $AuCl_3$ and either pyridine or bipyridine in aqueous ethanol was heated for 1 h at 60 °C. The reaction mixture was cooled to room temperature, and the solvent was removed by evaporation on a vacuum line. The residue was washed with hot ether, and then recrystallized from ethanol giving powder product. The isolated complex was left to dry under vacuum for 5–6 h.

AuPy: $C_5H_5NCl_3Au$: Light orange. M.Wt.=382.43. Yield: 67%. Elemental analysis, Found (Calc.): % C = 15.67 (15.70); % H = 1.36 (1.32); % N = 3.62 (3.66); % Cl = 27.79 (27.81). Mass spectrometry (m/z)=383 $[P]^+$.

AuBpy: $C_{10}H_8N_2Cl_3Au$: Light orange. M.Wt.=459.52. Yield: 72%. Elemental analysis, Found (Calc.): % C = 25.91 (26.14); % H = 1.82 (1.76); % N = 5.96 (6.10); % Cl = 23.00 (23.15). Mass spectrometry (m/z)=425 $[P–Cl]^+$.

2.3. Biological assay

2.3.1. Biological activity

In vitro antibacterial and antifungal activity of the synthesized complexes were tested against the two bacteria: *Escherchia coli* as gram-negative bacteria and *Staphylococcus aureus* as gram-positive bacteria, and the two fungi: *Aspergillus flavus and Candida albicans*. The tests were carried out using paper disk diffusion method (The Central Lab, Ain Shams University). The detailed procedure was previously reported.[3,4] The obtained data were compared with those of the two standards: tetracycline antibacterial agent and Amphotericin B antifungal agent.

2.3.2. In vitro cytotoxicity studies

Three human cancer cell lines were used for the *in vitro* screening experiments: two breast cancer cell lines (MCF7 and T47D) and human liver carcinoma cell line (HepG2). Screening tests were carried out in the National Cancer Institute, Cairo University, Egypt. Complete and detailed procedure is previously reported.[3,4]

2.3.3. Fluorescence quenching measurements

DNA competitive binding studies with ethidium bromide solution (EB) were carried out at different concentrations ranged from 1.0 M to 8.0×10^{-5} M. The concentrations of EB and Calf thymus-DNA (CT-DNA) were kept constant at 1.0×10^{-5} M. Before measurements, the resulting solutions were shaken up and incubated for 30 min. All the samples

were excited at 510 nm and the emission spectra were recorded in the wavelength range of 540–680 nm. The quenching constant (K_{sv}) was calculated using the Stern–Volmer equation[22]:

$$\frac{I_o}{I} = I + K_{sv}[\text{complex}]$$

where I_o and I are the fluorescence intensities in absence and presence of the quencher (complex). The K_{sv} value was obtained from the slope of the plot of I_o/I versus complex concentrations.

2.3.4. Viscosity measurements

Viscosity experiments were performed using Ostwald viscometer immersed in a water bath at a constant temperature (30.0 ± 0.1 °C). CT-DNA samples of approximately 0.5 mM were prepared by sonication in order to minimize complexities arising from CT-DNA flexibility. Flow time was measured with an automated timer three times for each sample and an average flow time was calculated. Data were presented as $(\eta/\eta_o)^{1/3}$ versus the ratio [complex]/[DNA]; η and η_o are the viscosities of the CT-DNA solution in presence and absence of the complex. Viscosity values were calculated after correcting the flow time of buffer alone (t_o), $\eta=(t-t_o)/t_o$.

2.4. Computational details

All the calculations were performed using the hybrid density functional theory (DFT) method B3LYP as implemented in the Gaussian 09 software package.[23] The geometries were optimized using the standard double zeta plus polarization basis set 6–31G (d,p) for ligands atoms and effective core potential basis set LANL2DZ for metal complexes. The purpose of the quantum mechanics calculations validates the proposed 3D structure of the obtained complexes as well as to find out key factors for their reactivity. The theoretical calculations of the spectral modes of vibrations were carried out using DFT and MP2 methods.

3. Results and discussion

3.1. Spectroscopic studies

Three gold(III) complexes were isolated from the reactions of 2-pyrazinecarboxamide (**PCA**), pyridine (**Py**) or bipyridine (**Bpy**) with molecular formulas [Au(PCA)Cl2]Cl, **AuPCA**, [Au(Py)Cl3], **AuPy** and [Au(Bpy)Cl2]Cl, **AuBpy**, Figure 2. The structures of the complexes were characterized using elemental analysis, mass, IR, Raman, ^{1}HNMR spectrometry as well as thermogravimetry (TG) technique. The ionized and total chloride contents of the complexes were determined potentiometrically using silver ion electrode. The color, yield, elemental analysis and mass spectrometry data of the complexes are given in the Experimental section. The fragmentation patterns in the mass spectra of the complexes along with the thermal analysis as well as the elemental analysis data revealed the correctness of the suggested

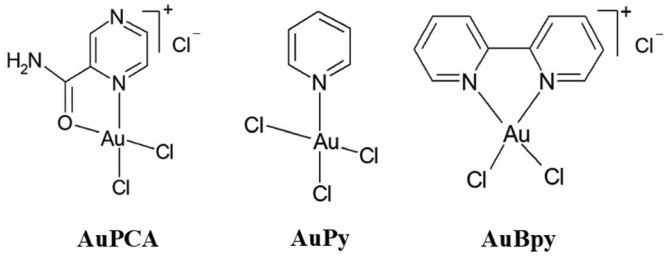

Figure 2. The proposed structures of the complexes.

molecular formulas. The electrical molar conductance in DMSO at room temperature for the two complexes **AuPCA** and **AuBpy** exhibited high molar conductance (125.5–136.4 μS) due to their electrolytic characteristics, while the molar conductance of **AuPy** was in the 21–25 μS range, which indicated that it is nonelectrolyte.

The IR and Raman spectra of **AuPCA** complex are shown in Figures 1S and 2S, and the data are tabulated in Table 1. The IR spectrum of **PCA** which is similar to Favipiravir drug without OH and F atom showed characteristic bands due to $\nu_{as}NH_2$ and ν_sNH_2 at 3413 and 3160 cm^{-1}, respectively, Table 1.[8,24] The vibration modes δNH_2, $\nu C{=}O$, $\nu C{-}N$, rNH_2 and τNH_2 were found at 1713, 1610, 1438, 1087, 618 cm^{-1}, respectively. It is interesting to note that chelation reverses the $\nu C{=}O$ and δNH_2 vibrations. The in-phase out of plane γCH was observed at 787 cm^{-1}, with medium intensity in comparison with pyrazine molecule.[25] The other infrared bands corresponded to skeletal vibrations of the pyrazine ring involving coupled C=C and C=N stretches and CH bends were observed in the wavenumber range 1600–1400 and 1400–1100 cm^{-1}. As expected, the CO stretch and NH_2 scissor of PCA were changed to lower wavenumbers due to complex formation since these coordinates are coupled.[26,27] The lowering from 1713 to 1660 cm^{-1} in the IR spectrum indicated that metal–oxygen stretch link is relatively strong. The other bands of pyrazine ring of **PCA** were also altered since gold ion is linked to the nitrogen of pyrazine ring as well as the CO group via the oxygen atom. The metal–ligand stretches were observed as new bands in the Raman spectra with medium intensity. The density functional theory (DFT) and the Møller–Plesset perturbation theory (MP2) calculations for the 45 vibrations expected for the **AuPCA** complex using Gaussian 09 software were used to assign the experimental wavenumbers based on the IR intensity, activity and depolarization ratio in the Raman spectra. In $LAuCl_3$-type compounds for C_1 symmetry, the three AuCl stretching modes or the bending modes are all active. The Au–Cl and Au–N coupled motions were calculated and observed at lower frequencies as given in Table 1. Bending vibrations of $AuCl_3$ were observed at lower wavenumbers by comparing with the stretching modes.[28,29] The assignments of in-plane (ip) and out of plane (oop) modes were also based on the calculated intensity and polarization of each vibration. Calculation indicated that oop modes are depolarized whereas the in-plane vibrations were polarized. It is interesting to note that vibrations at lower frequencies in the Raman spectra were enhanced

Table 1. Infrared and Raman spectral bands of **AuPCA** complex and their assignments based on DFT and MP2 calculations.

Vibration number	Measured IR of **PCA** (cm^{-1})	Observed Raman of **PCA** (cm^{-1})	Measured IR for **AuPCA** (cm^{-1})	Observed Raman for (**AuPCA**) (cm^{-1})	DFT calculation for **AuPCA** (C_1 point group)	MP2 calculation for **AuPCA**	Assignment of **AuPCA** vibrations
1	3413s	–	3450w	–	3705	3686	$\nu_a NH_2$
2	3290s	–	–	3162vw	3561	3534	$\nu_s NH_2$
3	3116m	–	–	3097vw	3263	3252	νCH
4	–	–	–	–	–	3232	νCH
5	–	–	–	3019vw	–	3215	νCH
6	1713vs	1674 w	1660vs	1660vw	1701	1720	δ NH_2, νC=O
7	1610m	1601vw	1581m	1591m	1600	1591	νC=O, δ NH
	1579m	1578s		1547w	1575	1563	ν_{ring}
8				1536	1559		ν_{ring}
9	1524w	1525m	1531w			1485	
10	1476w		1464w	1468w	1500	1479	ν_{ring}, δCH_{ring}
11	1438w		1421m	1422W	1456	1437	νC–$C_{chelate}$, νC–NH_2, ν_{ring}, δCH_{ring}
12	1378s		1380vw	1383w	1421	1393	ν_{ring}, δCH_{ring}
13		1322 w	1347s	1354w	1349	1332	δCH_{ring}, ν_{ring}
14			1283M	1288W	1264	1250	ν_{ring}
15	1182 m	1181w	1183m	1195W	1202	1183	δCH_{ring}, ν_{ring}
16	1164m	1170w	1160m	1171W	1186	1151	δCH_{ring}
17	1087m	1080w	1063m	1064	1099	1109	rNH2, νCO
18	1053s	1052m	1040m	1049w	1061	1050	ν_{ring}, δCH
19	1023s	1025m		–	1048	1007	δ_{ring}
20			958vw	–	1026	907	γCH
21	870m	868w	853m	–	963	895	γCH
22			820vw	854	897	834	γCH
23		807m	794w	–	811	784	γNH_2
24	787m	778w	764m	–	801	781	δ_{ring}
25	761vw		748sh, m	748m	781	748	γ_{ring}
26	699vw		685vw	675w	695	679	δNCO + δAu–O = $C_{chelate}$, δ_{ring}
27	670m	661w	673vw	675w	688	678	γO = C, γ ring
28	618w	618w	–	–	654	651	δ_{ring}, δNCO + $\delta_{chelate}$
29	543s		578m	574vw	565	559	τNH2
30	519s		–	515s	510	502	$\delta C_{chelate}$ $C_{Ring}O + \delta_{chelate}$
31		501br, w	–	502m	492	471	γ_{ring}
32			472m	473w	463	452	νAu–O
33			–	378s	373	357	$\nu_{as} AuCl_2$
34			–	332w	353	356	γ_{ring}
35			–	332w	353	351	$\nu_s AuCl_2$
36			–	299m	283	280	νAu–N, δN–$C_{chelate}$–C
37			–	239 m	250	251	δN–$C_{chelate}$–C
38			–	205w	198	201	$\delta_{chelate}$
39		181m	–	–	196	191	τC=O
40			–	162s	160	161	τC–C_{Ring}
41			–	127m	132	134	$\delta s AuCl_2$
42			–	–	110	104	γC–NH_2, γ_{ring}
43			–	99 m	103	103	r$AuCl_2$
44			–	–	63	63	w$AuCl_2$
45			–	–	50	49	$\tau AuCl_2$

ν, stretch; δ, in-plane bend, γ, out of plane bend; r, rocking; τ, torsion; s, symmetric; as, asymmetric.

Table 2. Infrared spectral bands of **AuPy** complex and their assignments based on DFT calculations.

Vibration number	Measured IR for **AuPy** (cm^{-1})	DFT Calc. for **AuPy**	Assignment of **AuPy** vibrations
1	3104	–	νCH
2	3080	–	νCH
3	3050	–	νCH
4	3031	–	νCH
5	–	–	νCH
6	1614vs	1650	ν_{ring}, δCH
7	1577m	1612	ν_{ring}, δCH
8	1483w	1516	ν_{ring}, δCH
9	1455vs	1490	ν_{ring}, δCH
10	1372m	1407	δCH in phase
11	1285w	1322	ν_{ring}
12	1211w	1264	ν_{ring}
13	1186mw	1207	δCH
14	1074s	1107	δCH
15	1067m	1091	δCH
16	1049w	1066	δ_{ring}
17	1049w	1056	δCH
18	1019m	1031	δ_{ring}
19	980v	1023	γCH
20	946w	992	γCH
21	–	903	γCH
22	759 s	795	γCH in phase
23	682s	716	γCH
24	660sh	670	δ_{ring}
25	–	662	δ_{ring}
26	474m	465	γ_{ring}
27	423vw	407	γ_{ring}
28	–	335	ν_{as} $AuCl_{2trans}$, δAuNC
29	–	335	ν_{as} AuClN, δClAuN,

ν, stretch; δ, in-plane bend, γ, out of plane bend; r, rocking; τ, torsion; s, symmetric; as, asymmetric.

due to complex formation, which may give these bands some analytical significance.

The measured IR wavenumbers of **AuPy**, **Bpy** and **AuBpy** and the assignment of the frequencies using DFT method are tabulated in Tables 2 and 3. Figure 3S gives the measured and calculated IR spectra of **AuBpy**. As can be noticed, the experimental and calculated stretching in-plane (ip) and out of plane bending vibrations (oop) were existed at higher wavenumbers up to around 400 cm^{-1}. The vibrations around 1600 cm^{-1} represented coupled ring stretch vibrations. Below 400 cm^{-1}, the vibrations of the chelating ring and $AuCl_2$ stretching and bending modes were assigned based on DFT calculation and by comparison with previous experimental and calculation work.[30] The 5 γCH vibrations expected for pyridine were found below 1000 cm^{-1} till up to 700 cm^{-1} with two intense characteristic bands at 759 and 682 cm^{-1}. For **AuBpy** complex with a C_s symmetry, its vibrations were located at the same wavenumber zones as for **AuPy**, which has a tetrahedral structure (Tables 2 and 3). In-plane vibrations were of A' type whereas out of plane vibrations were of A" symmetry. The vibrations of the complexed part are different since their symmetries are different. The characteristic modes of higher intensity occurred at 768, 1449 and 1600 cm^{-1} for the **AuBpy** complex, whereas the calculated were at 825, 1520 and 1758 cm^{-1}. These values corresponded to in phase out of plane (oop) CH bend, coupled ring stretch, CH bend, and ring stretch, respectively. The modes of $AuCl_3$, $AuCl_2$ and for chelating rings were found below 400 cm^{-1}. Below 400 cm^{-1}, stretching and bending modes of $AuCl_2$ were observed as expected by comparison with numerous previous experimental data.[31,32]

The 1H and 13C (H-decoupled) NMR spectra of the reported gold complexes gave more insight on their structure. Figure 3 illustrates the ^{1}H NMR spectra the two complexes AuPCA and **AuBpy**, while Table 4 gives all the spectral data. All the spectra performed signals due to protons of the coordinated ligands.[8,26] From the IR and NMR studies, it can be concluded that the present gold(III) complexes formed only square planer binary derivatives. The 1H NMR spectrum of **AuPCA** complex displayed signals due the **PCA** ligand only, while the other two complexes, **AuPy** and **AuBpy** showed that the gold ion coordinated solely to either pyridine or bipyridine ligand (Figure 3; Table 4). Interestingly, platinum(II) and platinum(IV) gave ternary complexes with pyrazinecarboxamide and either pyridine or bipyridine.[8,33] This could be due to the higher charge density and lower ionic size of the gold ions relative to the platinum(II) ones. Also, the prevalence of the formation of the pyridine or bipyridine gold complexes over the expected ternary complexes could be revealed from the different charge values on the nitrogen atoms of the three ligands (Hückel molecular orbital calculation), Figure 1. In case of Pt(IV) derivatives, the formation of the ternary complexes was also facile due to octahedral configuration.[8,33] Therefore, according to the spectroscopic, analytical and physical results, we suggest that the ligands coordinated to the gold species to give square planar structures as illustrated in Figure 2. The elucidated structure of **AuBpy** complex is analogous to that found for 1,2-dichloro(*o*-phenanthroline)gold(III) chloride.[34] Also, the **AuPy** complex is consistent to that found by X-ray study for the complex.[35]

3.2. Thermal analysis

Thermogravimetric (TG) studies were carried out to examine the thermal stability of the gold complexes.[36] The TG

Table 3. Infrared spectral bands of **AuBpy** complex and their assignments based on DFT calculations.

Vibration number	Measured IR of **Bpy** (cm^{-1})	Measured IR of **AuBpy** (cm^{-1})	DFT calc. for **AuBpy** (C_s point group)	Assignment of **AuBpy** vibrations
1		3200w	3269	νCH
2		3138vw	3269	νCH
3		3110w	3058	νCH
4	3086 w	3081 m	3054	νCH
5	3053 w	3056w	3050	νCH
6		sh, w	3048	νCH
7		sh, w	3040	νCH
8		sh, w	3037	νCH
9	1578s	1600s	1758	ν_{ring} A″
10	1555 m	1566w	1632	ν_{ring}, δCH A′
11		–	1627	ν_{ring} A″
12		1566s	1603	ν_{ring} A″
13	1490w	1500s	1600	ν_{ring} A′
14	1454 vs	1467m	1530	ν_{ring}, δCH A′
15		1449s	1491	ν_{ring}, δCH A″
16		–	1476	ν_{ring} A′
17	1415 m	1419m	1459	ν_{ring} A′
18		–	1364	ν_{ring} A′
19		1311s	1352	ν_{ring} A″
20		1300sh	1341	ν_{ring} A′
21	1249 m	1249s	1311	δCH A″
22	1210 w	1198w	1304	δCH A′
23		1179	1223	δCH A′
24	1167 wbr	1159w	1216	δCH A″
25	1137 w	1123w	1154	δCH A″
26	1086 w	1108m	1131	δCH A′
27	1062 m	1069m	1088	δCH A″
28	1038 m	1045w	1075	δCH A′
29	–	1027m	1058	δ_{ring} A′
30		–	1055	γCH A″
31	991 m	1000w	1048	γCH A″
32		–	1046	γ_{ring} A′
33		–	1016	γCH A′
34		–	1013	γ_{ring} A″
35		–	1009	γCH A″
36		892vw	922	γCH A′
37	891 w	–	907	γCH A″
38		795vw	825	γ_{ring} A′
39	758 vs	768vs	804	γCH in phase A″
40		–	774	δ_{ring} A′
41		706m	740	γCH, γ_{ring} A′
42		675w	710	γ_{ring} A″
43	651 m	659m	683	δ_{ring} A′
44		vw band	657	δ_{ring} A″
45	617m	vw band	651	δ_{ring}, $\nu_{as}AuN_2$ A″
46		539vw	562	γ_{twist} inter-ring A″
47		486w	473	δ inter-ring A″
48	428w	439m	463	γ_{wag} inter-ring A″
49		409w	432	γ_{ring} A′
50		–	369	δ inter-ring A′
51		–	356	τ inter-ring A″
52		–	292	ν_sAuCl_2, A′
53		–	255	δ chelated ring, ν_sAuCl_2 A′

ν, stretch; δ, in-plane bend, γ, out of plane bend; r, rocking; τ, torsion; s, symmetric; as, asymmetric.

data of the complexes are tabulated in Table 5. The formulas of liberated fragments in the decomposition steps were suggested depending on the percentage mass loss. In addition, the formula of final residue was dependent on elemental analysis. The TG curve of **AuPCA** complex exhibited three (two overlapped and one resolved) decomposition steps. The first two steps at 186–377 °C, with a weight loss of 26.25%, could be attributed to the liberation of $^{C}2^{H}4+$ NCl2 moieties. The final step exhibited a weight loss of 19.12% and assigned to elimination of HOCl and N_2 moieties to leave AuC_3 species as a residue, % C found (calc.)=15.2 1). The TG plot of the **AuPy** complex showed two resolved decomposition steps within the temperature range 158–724 °C. The first step corresponded to the loss of Cl_2 species with a weight loss of 18.53%. The other decomposition step was assigned to the elimination of a C_5H_5NCl moiety to leave a metallic gold residue. The TG curve of **AuBpy** complex also illustrated two decomposition steps within the temperature range 111–648 °C. The first decomposition step corresponded to the loss of loss of Cl_2 species. The second step involved the loss of a bipyridine and a Cl species to give metallic gold as a residue.

According the thermogravimetric patterns of the investigated complexes, the thermal stability increases in the order **AuBpy** <**AuPy** < **AuPCA**.

3.3. Biological evaluation

3.3.1. Antibacterial and antifungal activities

The free ligands (**PCA** and **Bpy**) and the gold complexes were screened against *Escherchia coli* as Gram-negative bacteria and *Staphylococcus aureus* as Gram-positive bacteria as well as the two fungi *Aspergillus flavus* and *Candida albicans* to assess their potential activity relative to the two standards: Tetracycline antibacterial agent and Amphotericin B antifungal agent, Table 6. The data showed that the free ligands have the capacity of inhibiting the metabolic growth of the investigated bacteria and the fungi to different extents, which may indicate broad-spectrum properties; especially for the **Bpy** ligand. The activity of these compounds may arise from the presence of NH, C=N and C=O groups. The mode of action may involve formation of hydrogen bonding between those functional groups and the active centers of the cell constituents, leading to interference with the normal cell process.[37,38] The gold complexes showed some activities against both *Escherichia coli* and *Staphylococcus aureus* bacteria, but they were less than Tetracycline standard. On the other hand, the complexes showed better antifungal activities against the fungus *Candida albicans* with comparison to the fungus *Aspergillus flavus*. Activity of the metal complexes could be related to the lipophilic nature of the complexes, which arose from the chelation pattern. It was also noted that the toxicity of the metal complexes increases with increasing the concentration. This elevation is probably due to faster diffusion of the chelates through the cell membrane. The chelated derivatives may block the enzymatic activity of the cell or it may catalyze the toxic reactions among cellular constituents.[37,38] It is worth to mention that the biological activity of the ligands was better than those of complexes, i.e., complexation did not improve the activity. However, *in vivo* studies are required in this case to differentiate between the toxicity and activity of the compounds.

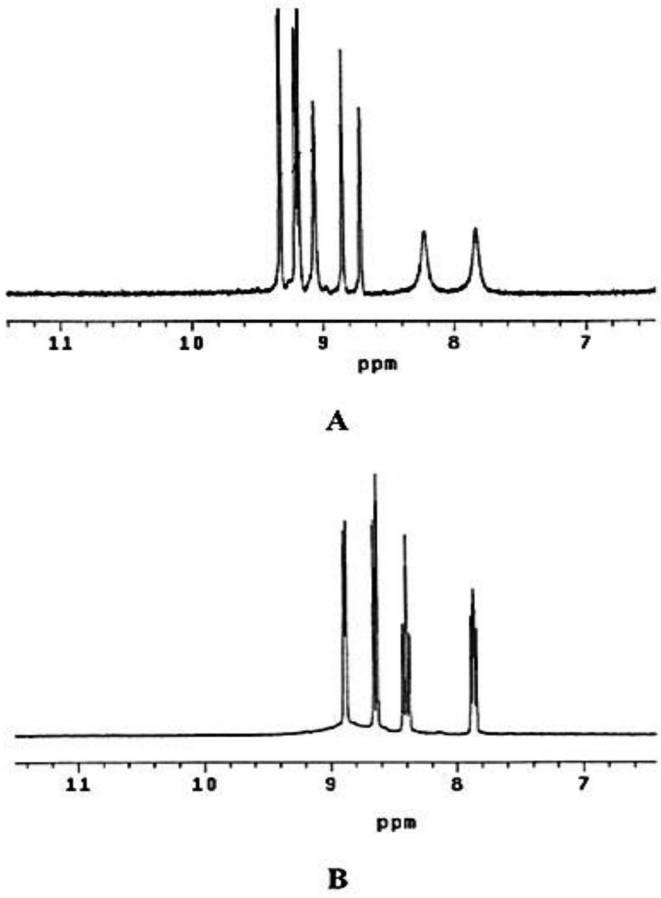

Figure 3. The ^{1}H NMR spectrum of **A**, **AuPCA** complex; **B**, **AuBpy** complex.

3.3.2. Cytotoxicity studies

To evaluate the potential usefulness of the **PCA** ligand and the reported gold complexes as antitumor agents, three human cell lines (two breast cancer cell lines, MCF7 and T47D, and a liver carcinoma cell line, HepG2) were treated by the compounds and compared with *cis*-platin activity as a standard. The complexes showed reasonable activities against the studied cell lines, which were better than the **PCA** ligand. The IC_{50} values (concentration that produce 50% inhibition of cell growth) of **PCA** ligand and the complexes as well as those of the *cis*-platin were determined and given in Table 7. The IC_{50} values of the compounds

Table 4. The ^{1}H and ^{13}C NMR data for the **PCA** ligand and the gold complexes.

Compound	^{1}H NMR data (ppm)	^{13}C NMR data (ppm)
PCA	9.28 (d, 1 Hz, Pz–CH), 8.95 (d, 8 Hz, Pz–CH), 8.81 (dd, 8, 1 Hz, Pz–CH), 8.42 (bs, NH), 8.02 (bs, NH).	161.79 (s, C=O), 146.01 (s, Pz–C), 145.03 (s, Pz–C), 144.65 (s, Pz–C), 144.69 (s, Pz–C)
AuPCA	9.33 (d, 1 Hz, Pz–CH), 9.13 (d, 8 Hz, Pz–CH), 8.65 (dd, 8, 1 Hz, Pz–CH), 8.23 (bs, NH), 7.83 (bs, NH).	162.15 (s, C=O), 153.70 (s, Pz–C), 144.76 (s, Pz–C), 144.52 (s, Pz–C), 141.19 (s, Pz–C)
AuPy	9.29 (m, Py–CH), 8.95 (m, Py–CH), 8.65 (m, Py–CH), 8.13 (m, Py–CH).	149.8 (s, Py–C), 137.8 (s, Py–C), 121.9 (s, Py–C)
AuBpy	8.88 (m, Py–CH), 8.65 (m, Py–CH), 8.40 (m, Py–CH), 7.87 (m, Py–CH).	157.4 (s, Bpy2 and 2′-C), 150.0 (s, Bpy–C), 137.2 (s, Bpy–C), 124.2 (s, Bpy–C), 120.8 (s, Bpy–C)

Table 5. Thermal analysis data for the gold complexes.

Molecular formula	Molecular weight	Decomposition temperature (°C)	% Weight loss	Eliminated species	% Solid decomposition residue
AuPCA	426.61	186–377	26.25	$NCl_2 + C_2H_4$	54.45
		378–705	19.12	$HOCl + N_2$	(AuC_3)
AuPy	382.60	158–261	18.53	Cl_2	51.49
		262–724	29.95	$C_5H_5N + 1/2\ Cl_2$	(Au)
AuBpy	459.52	111–393	15.45	Cl_2	42.86
		394–648	41.70	$C_{10}H_8N_2 + 1/2\ Cl_2$	(Au)

Table 6. *In vitro* antibacterial and antifungal activities of the gold complexes.

	Inhibition zone (mg/mm)			
Reagent	*Escherichia coli*	*Staphylococcus aureus*	*Aspergillus flavus*	*Candida albicans*
PCA	0	4	14	20
Bpy	14	13	35	28
AuPCA	8	6	4	14
AuPy	7	8	6	13
AuBpy	8	8	7	13
Tetracycline	30	27	–	–
Amphotericin B	–	–	14	20

Table 7. The IC_{50} values, μg/ml (mmol/L), of the gold complexes and *cis*-platin as a standard.

Complex	MCF7	T47D	HepG2
PCA	13.45 (10.92)	–	15.07 (12.24)
AuPCA	12.20 (28.60)	16.30 (38.22)	22.00 (51.59)
AuPy	16.60 (43.40)	16.30 (42.62)	23.50 (61.45)
AuBpy	15.50 (20.32)	9.23 (12.10)	17.90 (23.46)
cis-platin	5.71 (19.03)	–	3.67 (12.23)

qualitatively determine the strength of anticancer drug. Accordingly, the obtained IC_{50} values (ranged from 9 to 23 μg/ml) are considered due to intermediate anticancer reagents.[39,40] The increase of anticancer potency of the gold complexes over the ligand may be due to the metal atom, which is implicated by the chelation as suggested by Tweedy's chelation theory.[41] On chelation, the polarity of the metal ion is reduced to some extent due to the overlap of the ligand orbital and partial sharing of the positive charge of the metal ion with donor parts. In addition, it increases the delocalization of p electrons of the chelating ring and enhances the lipophilicity of the complexes, which enhances, in turn, the penetration of the complexes into lipid membranes and blocks the metal binding sites in the tumor. However, further *in vivo* studies on the activity of the complexes are required to evaluate the potency of these derivatives as antitumor reagents.

3.3.3. Fluorescence quenching studies

Fluorometric competitive binding experiments are widely used to investigate the interaction between small molecules and macromolecules such as protein and DNA.[42] Information about the binding properties of these small molecules to protein/DNA can be obtained, such as the binding mechanism, binding mode, binding constant, binding sites, and intermolecular distances.[43] Fluorescence quenching refers to any process that decreases the fluorescence intensity from a fluorophore induced by a variety of molecular interactions including excited-state reactions, molecular rearrangements, energy transfer, ground-state complex formation and collisional quenching.[44]

Ethidium bromide (EB) is used to investigate the potential DNA binding mode of many compounds. EB emits intense fluorescence at 608 nm in the presence of CT-DNA due to its strong intercalation between the adjacent DNA base pairs. The addition of a second molecule, which binds to DNA more strongly than EB would quench the DNA-induced EB emission.[45] The extent of quenching of the fluorescence of EB bound to DNA would reflect the extent of the DNA binding of the second molecule. The emission spectra of DNA-bound EB in the absence and the presence of different concentrations of the gold complexes are shown in Figures 4–6. It is clearly seen that the addition of the reported complexes to CT-DNA pretreated with EB caused an appreciable reduction in the emission intensity. These results indicated that the gold complexes bind to DNA at the sites occupied by EB itself. Fluorescence quenching can occur by different mechanisms, which are usually classified as dynamic and static quenching. The former may result from collision between the quencher and the fluorophore, while the latter could be due to the formation of a complex between the fluorophore and quencher.[46] The quenching plots in Figures 4–6, illustrate that the quenching of EB bound to CT-DNA by the gold complexes are in good agreement with the linear Stern–Volmer equation. The K_{sv} values are: **AuBpy**$=0.93\times10^{4}$, **AuPy**$=0.75\times10^{-4}$ and **AuPCA**$=2.25\times10^{4}$.

3.3.4. Viscosity measurements

In order to further investigate the interaction mode between the gold complexes and CT-DNA, viscosity measurements were carried out to clarify the effect of interaction on the length of CT-DNA (Figure 7). Although optical photophysical probes usually offer essential information about the binding modes of complexes to DNA, they are lacking certain evidences to support an intercalative binding model.[47] In the absence of crystallographic structure data, hydrodynamic methods, which are sensitive to the change of DNA length, are regarded as the least ambiguous and most critical tests of binding in solutions. Intercalating agents are expected to be increased in the relative specific viscosity $(\eta/\eta_o)^{1/3}$ of CT-DNA. This is due to elongation of the double helix to accommodate the compounds in-between the base pairs. The plots of the relative viscosity $(\eta/\eta_o)^{1/3}$ versus R, R= [Complex]/[DNA], showed a significant increase in the relative specific viscosity of DNA solution with increasing the concentration of complexes. This indicates that complexes bind to CT-DNA through an intercalation-binding mode.[48] The classical intercalators like ethidium bromide are known to increase the base pair separation resulting in an increase in the relative viscosity of the CT-DNA. The effect of the gold complexes is far less than that observed for the EB intercalator, which indicates that the existence of a weak intercalative interaction between the complexes and CT-DNA. Therefore, it can be concluded that the gold complexes exhibited high binding extent with CT-DNA. The increased degree of viscosity, which may depend on its

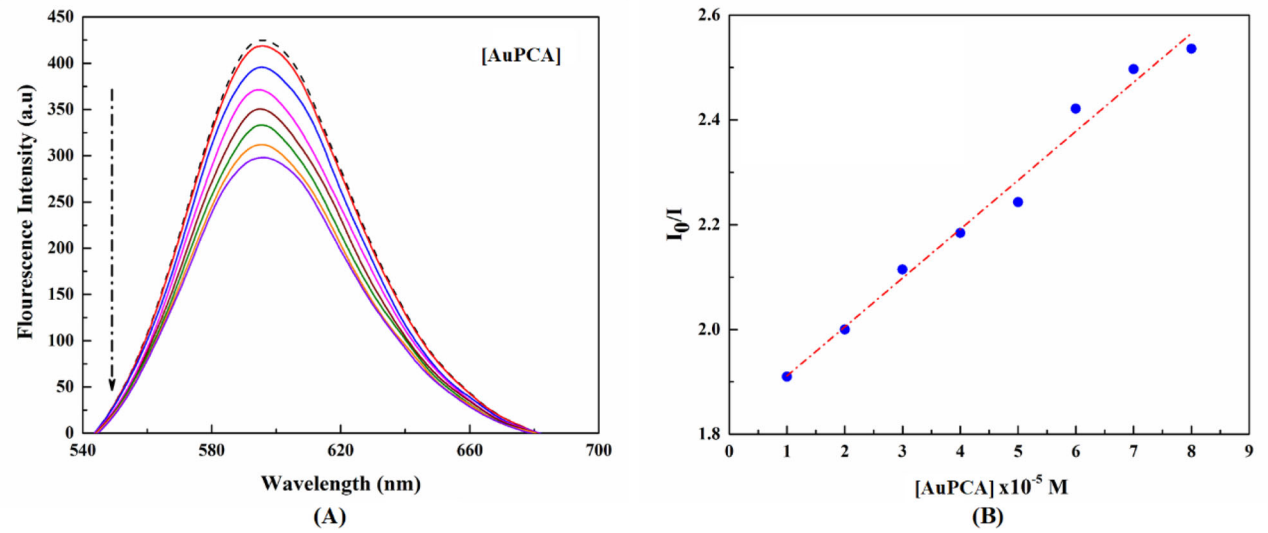

Figure 4. (**A**) Fluorescence emission spectra of EB–DNA system in absence (dashed line) and presence (solid line) of **AuPCA** complex; arrow indicates the intensity changes upon increasing concentration of complex. (**B**) Fluorescence variation profile of **AuPCA** complex versus molar concentration.

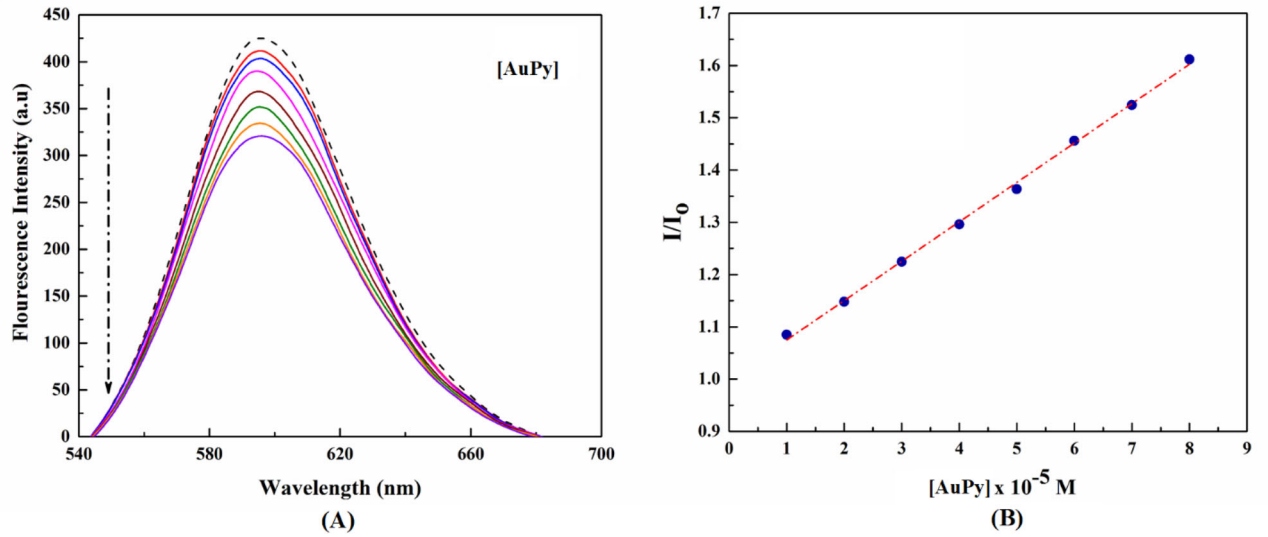

Figure 5. (**A**) Fluorescence emission spectra of EB–DNA system in absence (dashed line) and presence (solid line) of **AuPy** complex; arrow indicates the intensity changes upon increasing concentration of complex. (**B**) Fluorescence variation profile of **AuPy** complex versus molar concentration.

affinity to DNA, follows the order of **AuBpy** >**AuPy** >**AuPCA**. Obviously, this is consistent with the foregoing conclusion suggested from the fluorescence quenching data. The results of DNA binding studies indicated that the suggested mechanism for interaction between the gold complexes and DNA was via an intercalative mode.

3.4. The stereochemistry and chemical reactivity prediction

The stereochemistry of the reported gold complexes was investigated by the hybrid density functional theory (DFT) method. According to the analytical and spectroscopic investigations, the gold complexes have the molecular formulas [Au(PCA)Cl2]+, [Au(Py)Cl3] and [Au(Bpy)Cl2]+. Optimized structures of these complexes (Figure 8) showed that they have square planar arrangements with total minimized energy = 21.74, 10.11, and 22.98 kcal/mol, respectively. The structure of **AuPCA** is almost planar with a dihedral angle C_1–N_7–Au_{16}–Cl_{14} equal to 179.9°. Also, the two bond angles N_7–Au_{16}–O_9 and Cl_{14}–Au_{16}–Cl_{15} were found to be 78.0° and 89.1° indicating a distorted square planar coordination around the metal. In addition, the bond angle O_9–Au_{16}–Cl_{14} approaches the linearity (175.2°). On the other hand, the bond lengths Cl_{14}–Au_{16}, N_7–Au_{16} and O_9–Au_{16} were found to be in the normal range (2.37, 2.13 and 2.12 Å).[35,49] In case of the **AuPy** complex, the optimized structure illustrated that gold existed in a regular square planar as indicated from the bond angles around Au (Cl_8–Au_{10}–Cl_{12}, 89.8°; Cl_9–Au_{10}–Cl_{12}, 89.9°; N_7–Au_{10}–Cl_{12}, 180.0° and Cl_8–Au_{10}–Cl_9, 179.7°). The bond lengths around the gold ion were found to be comparable to those observed for **AuPCA** complex. For example, Au_{10}–Cl_{12} and N_7–Au_{10} were found to be 2.38 and 2.10 Å, respectively and also with previously DFT and X-ray studies especially for Au–N bond, bond angles Cl–Au–Cl and N–Au–Cl, where the four angles

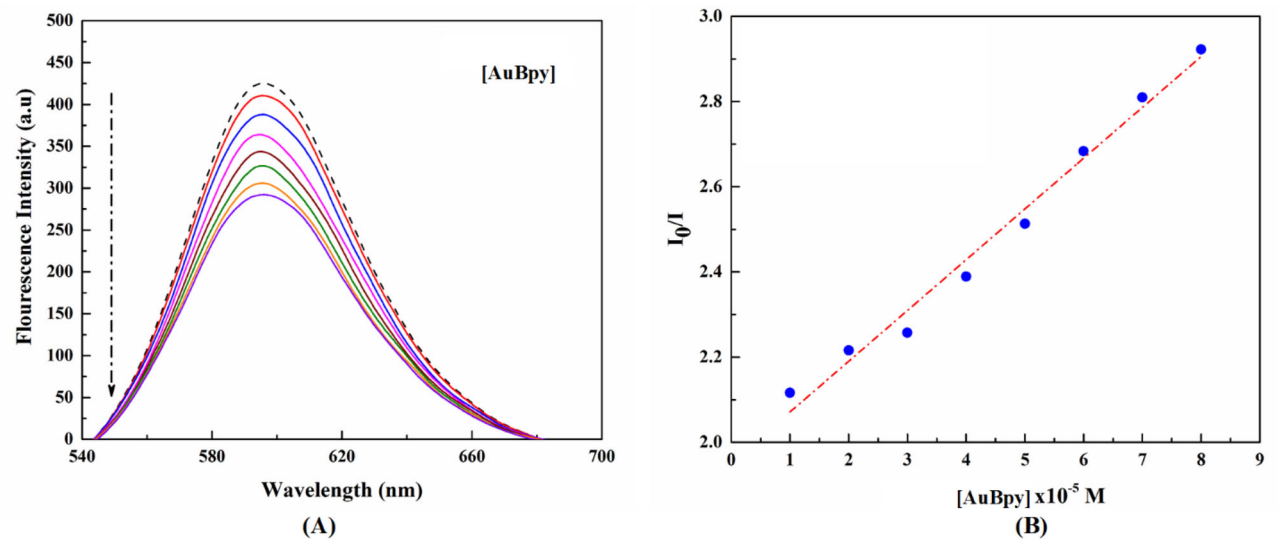

Figure 6. (**A**) Fluorescence emission spectra of EB–DNA system in absence (dashed line) and presence (solid line) of **AuBpy** complex; arrow indicates the intensity changes upon increasing concentration of complex. (**B**) Fluorescence variation profile of **AuBpy** complex versus molar concentration.

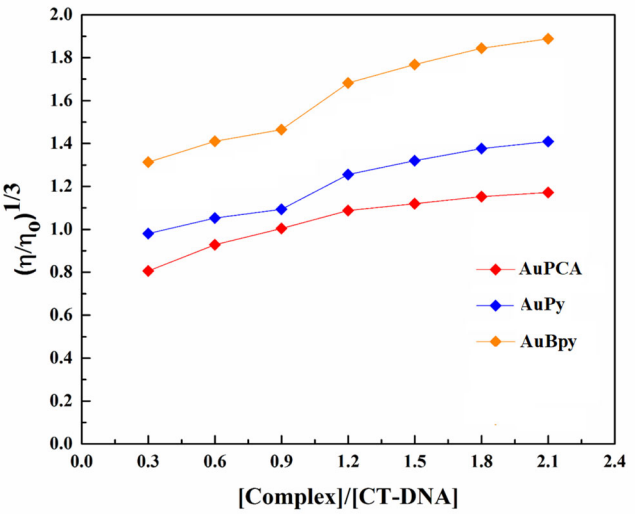

Figure 7. Effect of increasing concentrations of complexes on the relative viscosity of CT-DNA.

Cl–Au–Cl are 90° giving a symmetric square planar structure.[35]

The energetically minimized structure of **AuBpy** complex displayed large deviation from the square planar arrangements expected for gold complexes, Figure 8. The bond angles around the gold ion showed different values than those detected for the other two gold complexes. For example, the bond angles N_{22}–Au_3–N_{23}, Cl_1–Au_3–Cl_2, Cl_1–Au_3–N_{22} and Cl_2–Au_3–N_{23} have the values 78.1°, 93.7°, 123.28° and 120.9°, respectively. Interestingly, the bond lengths also showed different values than the other two complexes. The Au–Cl bond was elongated while the Au–N bond was shortened (Cl_1–Au_3, 2.50 Å; Cl_2–Au_3, 2.52 Å; Au_3–N_{22}, 2.09 Å and Au_3–N_{23}, 2.10 Å).[35,49]

The global chemical reactivity parameters including HOMO, LUMO, energy gap (ΔE), electronegativity (X), chemical potential (V), electron affinity (A), ionization potential (I), chemical hardness (η), chemical softness (S) and electrophilicity (ω) of the reported compounds are given in Table 8.[41,42] The frontier molecular orbital energies were estimated using DFT method (B3LYP) and illustrated in Figure 9 The HOMO orbital energy represents the electron donating ability, while the LUMO orbital energy characterizes the electron withdrawing ability. The energy gap between HOMO and LUMO shows the molecular chemical stability; it is a critical parameter for determining molecular electrical transport properties. Smaller energy gap reflects the easiness of the charge transfer (CT), and the polarization, which occurs within the molecule.[43,50,51] Therefore, the order of increasing reactivity of the reported complexes is: **AuBpy > AuPCA > AuPy**. Interestingly, the calculations revealed that the gold complexes have higher reactivity relative to the corresponding platinum derivatives.[33] In addition, the electronegativity parameter is a reflection for the electrostatic potential, where the electron partially transferred from one of lower electronegativity to another of higher electronegativity.[52] The results showed that the order of decreasing X is: **AuPCA > AuBpy > AuPy**. On the other hand, the results of small chemical hardness values for the reported derivatives reflect the ability of charge transfer within the molecule. The order of increasing the charge transfer within the molecule is: **AuPy < AuPCA < AuBpy**. Thus, the electronegativity and chemical hardness descriptors indicated that the gold complexes have better charge transfer ability than those of the platinum ones.[33] On the other hand, the binding energy was calculated using the following equation[53]:

$$BE = \frac{[aE_{Au} + bE_C + cE_H + dE_N + eE_o + fE_{Cl}] - [Ecomplex]}{a+b+c+d+e+f}$$

where a, b, c, d, e and f are the number of Au, C, H, N, O and Cl atoms and E_{Au}, E_C, E_H, E_N, E_O and E_{Cl} are the ground state total energies of Au, C, H, N, O and Cl atoms, respectively. $E_{complex}$ is the energy of optimized complex. As can be seen from Table 8 the order of increasing the binding energy of the complexes follows

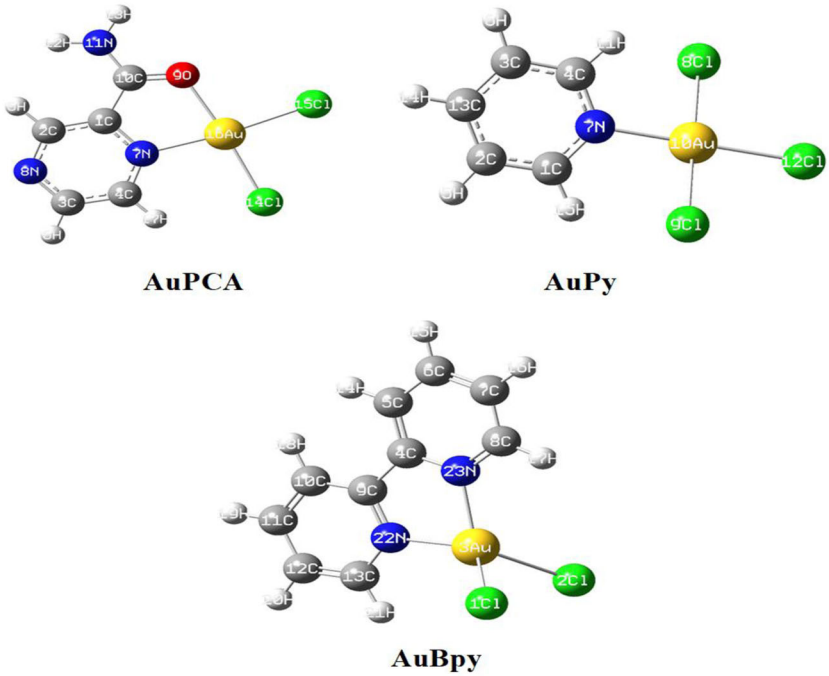

Figure 8. The optimized structures of gold complexes.

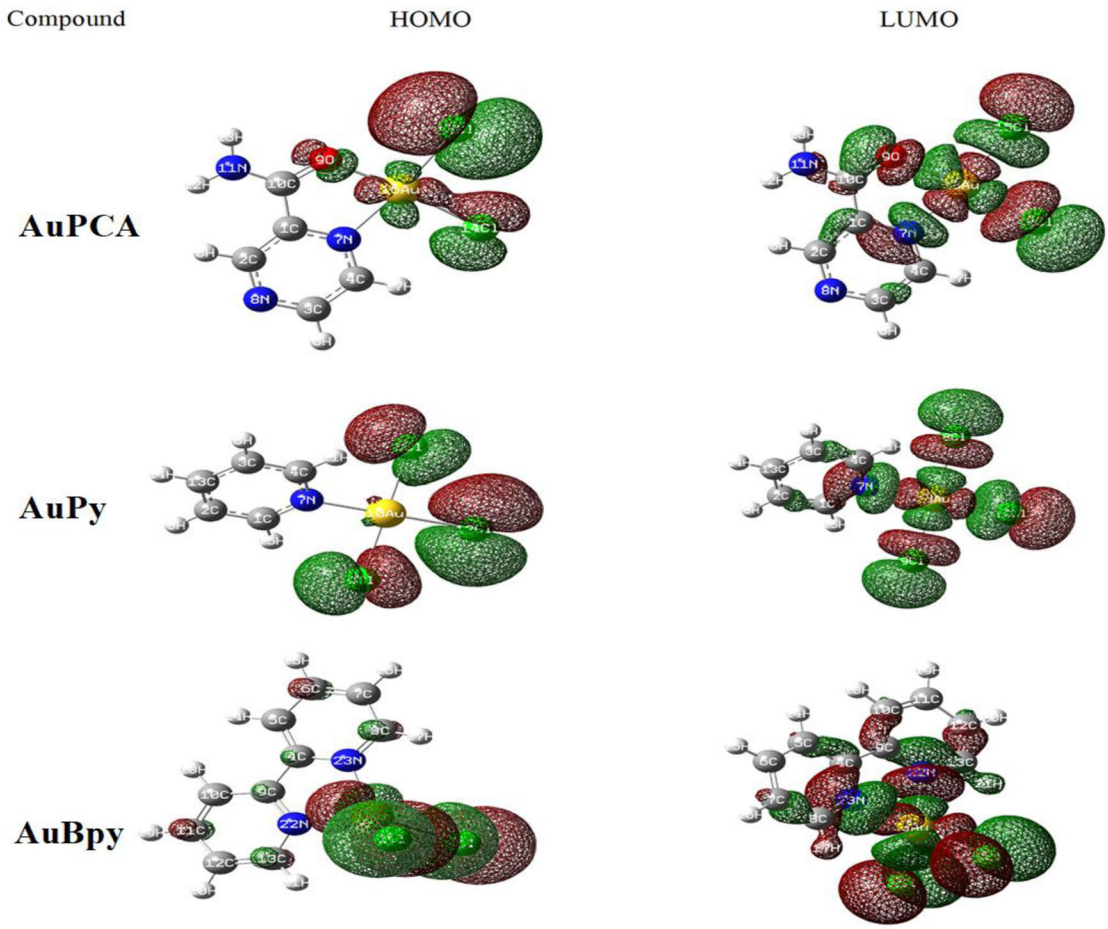

Figure 9. The frontier molecular orbitals of the gold complexes.

the order: **AuBpy < AuPy < AuPCA**. The calculated value of binding energy of **PCA** was found to be 11.99 eV, which is slightly higher than the corresponding complex (**AuPCA**). This might indicate that the stability of the formed complex is comparable with that of the free ligand.

Table 8. The global chemical reactivity descriptors for the gold complexes.

Parameter	AuPCA	AuPy	AuBpy
DM (Debye)	13.06	11.10	14.61
HOMO (eV)	−11.70	−7.55	−10.48
LUMO (eV)	−9.07	−4.80	−9.55
ΔE (eV)	2.62	2.75	0.93
X (eV)	10.38	6.17	10.02
V (eV)	−10.38	−6.17	−10.02
A (eV)	9.07	4.80	9.55
I (eV)	11.70	7.55	10.48
η (eV)	1.31	1.37	0.47
S (eV)	0.66	0.69	0.23
ω (eV)	41.09	13.85	107.81
BE (eV)	11.89	11.63	11.40

4. Conclusion

Three gold(III) complexes with heterocyclic nitrogen donor ligands were found to have interesting spectroscopic and structural features. The vibrational analysis of the ligands and their complexes in the ground state (using DFT and MP2) gave more insight on the appropriate assignments of the important functional groups of these types of complexes such as C=O, C=N, NH and Au–Cl. The reactivity and binding energies of the complexes, calculated from the frontier orbitals, were stemmed from the quantum global parameters. Cytotoxicity, fluorescence quenching and viscosity measurements of the gold complexes exhibited high binding extent with DNA. The results indicated that the suggested mechanism for interaction between the gold complexes and DNA was via an intercalative mode.

Supplementary Materials

Experimental and calculated IR and Rarman spectra (S1–S3) are provided as supplementary materials.

References

1. Wong, E.; Giandomenico, C. M. Current Status of Platinum-Based Antitumor Drugs. *Chem. Rev.* **1999**, *99*, 2451–2466. DOI: 10.1021/cr980420v.
2. Clarke, M. J. Ruthenium Metallopharmaceuticals. *Coord. Chem. Rev.* **2003**, *236*, 209–233. DOI: 10.1016/S0010-8545(02)00312-0.
3. Ramadan, R. M.; Abu Al-Nasr, A. K.; Noureldeen, A. F. H. Synthesis, Spectroscopic Studies, Antimicrobial Activities and Antitumor of a New Monodentate V-Shaped Schiff Base and its Transition Metal Complexes. *Spectrochim. Acta A Mol. Biomol. Spectrosc.* **2014**, *132*, 417–422. DOI: 10.1016/j.saa.2014.04.151.
4. Ramadan, R. M.; Elsheemy, W. M.; Hassan, N. S.; Abdel Aziz, A. A. Synthesis, Spectroscopic Characterization, Thermal Behavior and in vitro Antimicrobial and Anticancer Activities of Novel Ruthenium Tricarbonyl Complexes Containing Monodentate V-shaped Schiff Bases. *Appl. Organomet. Chem.* **2018**, *32*, 4180.
5. Bertrand, B.; Williams, M. R. M.; Bochmann, M. Gold(III) Complexes for Antitumor Applications: An Overview. *Chemistry* **2018**, *24*, 11840–11851. DOI: 10.1002/chem.201800981.
6. Kim, J. H.; Reeder, E.; Parkin, S.; Awuah, S. G. Gold(I/III)–Phosphine Complexes as Potent Antiproliferative Agents. *Sci. Rep.* **2019**, *9*, 12335. DOI: 10.1038/s41598-019-48584-5.
7. Holford, J.; Raynaud, F.; Murrer, B. A.; Grimaldi, K.; Hartley, J. A.; Abrams, M.; Kelland, L. R. Chemical, Biochemical and Pharmacological Activity of the Novel Sterically Hindered Platinum Co-Ordination Complex, *Cis*-[Amminedichloro(2-Methylpyridine)] Platinum(II) (AMD473). *Anticancer Drug Des.* **1998**, *13*, 1–18.
8. Ramadan, R. M.; Al-Raddady, N. S. Spectroscopic Studies, Biological Activity, and Cytotoxicity of Some Binary and Ternary Palladium and Platinum Complexes of Certain Heterocyclic Ligands. *Synth. React. Inorg. Met-Org. Nano-Met. Chem.* **2015**, *45*, 1183–1190. DOI: 10.1080/15533174.2013.862663.
9. Hay, M. ZD-0473 Johnson Matthey Plc. *Curr. Opin. Oncol. Endocr. Metab. Invest. Drugs* **1999**, *1*, 443.
10. Segapelo, T. V.; Guzei, I. A.; Spencer, L. C.; Van Zyl, W. E.; Darkwa, J. (Pyrazolylmethyl)Pyridine Platinum(II) and Gold(III) Complexes: Synthesis, Structures and Evaluation as Anticancer Agents. *Inorg. Chim. Acta* **2009**, *362*, 3314–3324. DOI: 10.1016/j.ica.2009.02.046.
11. Rubbiani, R.; Zehnder, T. N.; Mari, C.; Blacque, O.; Venkatesan, K.; Gasser, G. Anticancer Profile of a Series of Gold(III) (2-Phenyl)Pyridine Complexes. *ChemMedChem* **2014**, *9*, 2781–2790. DOI: 10.1002/cmdc.201402446.
12. Wang, S.; Shao, W.; Li, H.; Liu, Wang, C. K.; Zhang, J. Synthesis, Characterization and Cytotoxicity of the Gold(III) Complexes of 4,5-Dihydropyrazole-1-Carbothioamide Derivatives. *Eur. J. Med. Chem.* **2011**, *46*, 1914–1918. DOI: 10.1016/j.ejmech.2011.02.031.
13. Maiore, L.; Cinellu, M. A.; Nobili, S.; Landini, I.; Mini, E.; Gabbiani, C.; Messori, L. Gold(III) Complexes with 2-Substituted Pyridines as Experimental Anticancer Agents: Solution Behavior, Reactions with Model Proteins, Antiproliferative Properties. *J. Inorg. Biochem.* **2012**, *108*, 123–127. DOI: 10.1016/j.jinorgbio.2011.11.007.
14. Sun, L.; Chen, H.; Zhang, Z.; Yang, Q.; Tong, H.; Xu, A.; Wang, C. Synthesis and Cancer Cell Cytotoxicity of Water-Soluble Gold(III) Substituted Tetraarylporphyrin. *J. Inorg. Biochem.* **2012**, *108*, 47–52. DOI: 10.1016/j.jinorgbio.2011.12.003.
15. Al-Jaroudi, S. S.; Fettouhi, M.; Wazeer, I. M.; Isab, A. A.; Altuwaijri, S. Synthesis, Characterization and Cytotoxicity of New Gold(III) Complexes with 1,2-Diaminocyclohexane: Influence of Stereochemistry on Antitumor Activity. *Polyhedron* **2013**, *50*, 434–442. DOI: 10.1016/j.poly.2012.11.034.
16. Samanta, T.; Munda, R. N.; Roymahapatra, G.; Nandy, A.; Saha, K. D.; Al-Deyab, S. S.; Dinda, J. Silver(I), Gold(I) and Gold(III)-*N*-Heterocyclic Carbene Complexes of Naphthyl Substituted Annelated Ligand: Synthesis, Structure and Cytotoxicity. *J. Organomet. Chem.* **2015**, *791*, 183–191. DOI: 10.1016/j.jorganchem.2015.05.049.
17. Milacic, V.; Chen, D.; Ronconi, L.; Landis-Piwowar, K. R.; Fregona, D.; Dou, Q. P. A Novel Anticancer Gold(III) Dithiocarbamate Compound Inhibits the Activity of a Purified 20s Proteasome and 26s Proteasome in Human Breast Cancer Cell Cultures and Xenografts. *Cancer Res.* **2006**, *66*, 10478–10486. DOI: 10.1158/0008-5472.CAN-06-3017.
18. Che, C. M.; Sun, R. W.; Yu, W. Y.; Ko, C. B.; Zhu, N.; Sun, H. Gold(III) Porphyrins as a New Class of Anticancer Drugs: Cytotoxicity, DNA Binding and Induction of Apoptosis in Human Cervix Epithelioid Cancer Cells. Electronic Supplementary Information (ESI) Available: Further Experimental and Crystallographic Details. See http://www.rsc.org/suppdata/cc/b3/b303294a/. *Chem. Commun.* **2003**, *14*, 1718. DOI: 10.1039/b303294a.
19. Casini, A.; Cinellu, M. A.; Minghetti, G.; Gabbiani, C.; Coronnello, M.; Mini, E.; Messori, L. Structural and Solution Chemistry, Antiproliferative Effects, and DNA and Protein Binding Properties of a Series of Dinuclear Gold(III) Compounds with Bipyridyl Ligands. *J. Med. Chem.* **2006**, *49*, 5524–5531. DOI: 10.1021/jm060436a.
20. Marcon, G.; Carotti, S.; Coronnello, M.; Messori, L.; Mini, E.; Orioli, P.; Mazzei, T.; Cinellu, M. A.; Minghetti, G. Gold(III) Complexes with Bipyridyl Ligands: Solution Chemistry, Cytotoxicity, and DNA Binding Properties. *J. Med. Chem.* **2002**, *45*, 1672–1677. DOI: 10.1021/jm010997w.
21. Wang, Y.; He, Q. Y.; Sun, R. W.; Che, C. M.; Chiu, J. F. Cellular Pharmacological Properties of Gold(III) Porphyrin 1a, A

Potential Anticancer Drug Lead. *Eur. J. Pharmacol.* **2007**, *554*, 113–122. DOI: 10.1016/j.ejphar.2006.10.034.
22. Gehlen, M. H. The Centenary of the Stern–Volmer Equation of Fluorescence Quenching: From the Single Line Plot to the SV Quenching Map. *J. Photochem. Photobiol. C: Photochem. Rev.* **2020**, *42*, 100338. DOI: 10.1016/j.jphotochemrev.2019.100338.
23. Frisch, M. J.; Schlegel, H. B.; Scuseria, G. E.; Robb, M. A.; Cheeseman, J. R.; Scalmani, G.; Barone, V.; Mennucci, B.; Petersson, G. A.; Nakatsuji, H.; et al. Gaussian Inc., Wallingford, CT, **2009**.
24. Silverstein, R. M.; Bassler, G. C.; Morrill, T. C. *Spectrometric Identification of Organic Compounds*, 4th Edn.; Wiley: New York, **1991**.
25. Breda, S.; Reva, I. D.; Lapinski, L.; Nowak, M. J.; Fausto, R. Infrared Spectra of Pyrazine, Pyrimidine and Pyridazine in Solid Argon. *J. Mol. Struct.* **2006**, *786*, 193–206. DOI: 10.1016/j.molstruc.2005.09.010.
26. El-Medani, S. M.; Ali, O. A. M.; Mohamed, H. A.; Ramadan, R. M. Spectroscopic, Thermal and X-Ray Crystal Structure Studies of Some *Bis*-(Pyrazine-2-Carboxylato) Nickel(II) Complexes. *J. Coord. Chem.* **2005**, *58*, 1429–1437. DOI: 10.1080/00958970500156761.
27. Ramadan, R. M.; El-Medani, S. M.; Ali, O. A. M.; Mohamed, H. A. Spectroscopic and Thermal Studies of Some Palladium Complexes with Certain Heterocyclic Nitrogen Ligands. *J. Coord. Chem.* **2004**, *57*, 373–379. DOI: 10.1080/00958970410001680363.
28. Ferraro, J. R. *Low-Frequency Vibrations of Inorganic and Coordination Compounds*; Argonne National Laboratory: Argonne, Illinois; Plenum Press: New York, **1971**.
29. Liu, X. J.; Moritomo, Y.; Nakamura, A.; Kojima, N. Pressure-Induced Phase Transition in Mixed–Valence Gold Complexes Cs2Au2X6 (X = Cl and Br). *J. Chem. Phys.* **1999**, *110*, 9174–9178. DOI: 10.1063/1.478839.
30. Dollish, F. R.; Fateley, W. G.; Bentely, F. F. *Characteristic Raman Frequencies of Organic Compounds*; Wiley-Interscience Publication: New York, **1974**.
31. Brolo, A. G.; Jiang, Z.; Irish, D. E. The Orientation of 2,2′-Bipyridine Adsorbed at a SERS-Active Au(111) Electrode Surface. *J. Electroanal. Chem.* **2003**, *547*, 163–172. DOI: 10.1016/S0022-0728(03)00215-8.
32. Preda, N.; Mihut, L.; Baibarac, M.; Baltog, I.; Husanu, M.; Bucur, C.; Velula, T. Vibrational Properties of Polyaniline Functionalized PbI2. *Rom. J. Phys.* **2009**, *54*, 667.
33. Ramadan, R. M.; Abu Al-Nasr, A. K.; El-Medani, S. M. Synthesis, Spectroscopic and DFT Studies of Some Platinum-Pyrazine Carboxamide Derivatives. *J. Trans. Met. Complex.* **2018**, DOI: 10.32371/jtmc/236066.
34. Abbate, F.; Orioli, P.; Bruni, B.; Marcon, G.; Messori, L. Crystal Structure and Solution Chemistry of the Cytotoxic Complex 1,2-Dichloro(*O*-Phenanthroline)Gold(III) Chloride. *Inorg. Chim. Acta* **2000**, *311*, 1–5. DOI: 10.1016/S0020-1693(00)00299-1.
35. Radenkovic, S.; Antic, M.; Savic, N. D.; Glisic, B. D. The Nature of the Au-N Bond in Gold(III) Complexes with Aromatic Nitrogen-Containing Heterocycles: The Influence of Au(III) Ions on the Ligand Aromaticity. *New J. Chem.* **2017**, *41*, 12407.
36. Hatakeyama, T.; Liu, Z. *Handbook of Thermal Analysis*; Wiley: Chichester, UK, **1999**.
37. Harrold, M. W.; Zavod, R. M. *Basic Concepts in Medicinal Chemistry*; American Society for Health-System Pharmacists, **2013**.
38. Abdel Ghani, N. T.; Mansour, A. M. Structural and *In Vitro* Cytotoxicity Studies on 1H-Benzimidazol-2-ylmethyl-*N*-Phenyl amine and its Pd(II) and Pt(II) Complexes. *Spectrochim. Acta A Mol. Biomol. Spectrosc.* **2011**, *81*, 529–543. DOI: 10.1016/j.saa.2011.06.046.
39. Cutillas, N.; Yellol, G. S.; de Haro, C.; Vicente, C.; Rodríguez, V.; Ruiz, J. Anticancer Cyclometalated Complexes of Platinum Group Metals and Gold. *Coord. Chem. Rev.* **2013**, *257*, 2784–2797. DOI: 10.1016/j.ccr.2013.03.024.
40. Eckstein, N. Platinum Resistance in Breast and Ovarian Cancer Cell Lines. *J. Exp. Clin. Cancer. Res.* **2011**, *30*, 91. DOI: 10.1186/1756-9966-30-91.
41. Tweedy, B. G. Plant Extracts with Metal Ions as Potential Antimicrobial Agents. *Phytopathology* **1964**, *55*, 910.
42. Sirajuddin, M.; Ali, S.; Badshah, A. Drug–DNA Interactions and Their Study by UV–Visible, Fluorescence Spectroscopies and Cyclic Voltammetry. *J. Photochem. Photobiol. B.* **2013**, *124*, 1–19. DOI: 10.1016/j.jphotobiol.2013.03.013.
43. Zhang, J.; Wang, X. J.; Yan, Y. J.; Xiang, W. S. Comparative Studies on the Interaction of Genistein, 8-Chlorogenistein, and 3',8-Dichlorogenistein with Bovine Serum Albumin. *J. Agric. Food Chem.* **2011**, *59*, 7506–7513. DOI: 10.1021/jf2005194.
44. Sathyadevi, P.; Krishnamoorthy, P.; Alagesan, M.; Thanigaimani, K.; Muthiah, P. T.; Dharmaraj, N. Synthesis, Crystal Structure, Electrochemistry and Studies on Protein Binding, Antioxidant and Biocidal Activities of Ni(II) and Co(II) Hydrazone Complexes. *Polyhedron* **2012**, *31*, 294–306. DOI: 10.1016/j.poly.2011.09.021.
45. Liu, Z.-C.; Wang, B.-D.; Yang, Z.-Y.; Li, Y.; Qin, D.-D.; Li, T.-R. Synthesis, Crystal Structure, DNA Interaction and Antioxidant Activities of Two Novel Water-Soluble Cu^{2+} Complexes Derivated from 2-Oxo-Quinoline-3-Carbaldehyde Schiff-Bases. *Eur. J. Med. Chem.* **2009**, *44*, 4477–4484. DOI: 10.1016/j.ejmech.2009.06.009.
46. Samari, F.; Hemmateenejad, B.; Shamsipur, M.; Rashidi, M.; Samouei, H. Affinity of Two Novel Five-Coordinated Anticancer pt(II) Complexes to Human and Bovine Serum Albumins: A Spectroscopic Approach. *Inorg. Chem.* **2012**, *51*, 3454–3464. DOI: 10.1021/ic202141g.
47. Jia, L.; Jiang, P.; Xu, J.; Hao, Z. Y.; Xu, X. M.; Chen, L. H.; Wu, J. C.; Tang, N.; Wang, Q.; Vittal, J. J. Synthesis, Crystal Structures, DNA-Binding Properties, Cytotoxic and Antioxidation Activities of Several New Ternary Copper(II) Complexes of *N*,*N*′-(p-Xylylene)di-Alanine Acid and 1,10-Phenanthroline. *Inorg. Chim. Acta* **2010**, *363*, 855–865. DOI: 10.1016/j.ica.2009.12.047.
48. Anbu, S.; Kandaswamy, M.; Kamalraj, S.; Muthumarry, J.; Varghese, B. Phosphatase-Like Activity, DNA Binding, DNA Hydrolysis, Anticancer and Lactate Dehydrogenase Inhibition Activity Promoting by a New Bis-Phenanthroline Dicopper(II) Complex. *Dalton Trans.* **2011**, *40*, 7310–7318. DOI: 10.1039/c1dt10277j.
49. Zhu, S.; Gorski, W.; Powell, D. R.; Walmsley, J. A. Synthesis, Structures, and Electrochemistry of Gold(III) Ethylenediamine Complexes and Interactions with Guanosine 5'-Monophosphate. *Inorg. Chem.* **2006**, *45*, 2688–2694. DOI: 10.1021/ic051411p.
50. Raja, N.; Ramesh, R.; Liu, Y. Paramagnetic Ruthenium(III) Complexes Bearing *O*,*O* Chelating Ligands: Synthesis, Spectra, Molecular Structure and Electron Transfer Properties. *Polyhedron* **2012**, *31*, 196–201. DOI: 10.1016/j.poly.2011.09.019.
51. Chandra, S.; Gupta, L. K. Electronic, EPR, Magnetic and Mass Spectral Studies of Mono and Homo-Binuclear Co(II) and Cu(II) Complexes with a Novel Macrocyclic Ligand. *Spectrochim. Acta A Mol. Biomol. Spectrosc.* **2005**, *62*, 1102–1106. DOI: 10.1016/j.saa.2005.04.007.
52. Abdel Aziz, A. A.; Elantabli, F. M.; Moustafa, H.; El-Medani, S. M. Spectroscopic, DNA Binding Ability, Biological Activity, DFT Calculations and Non Linear Optical Properties (NLO) of Novel Co(II), Cu(II), Zn(II), Cd(II) and Hg(II) Complexes with ONS Schiff Base. *J. Mol. Struct.* **2017**, *1141*, 563–576. DOI: 10.1016/j.molstruc.2017.03.081.
53. Roohi, H.; Jahantab, M.; Yakta, M. Effect of the Stone–Wales (SW) Defect on the Response of BNNT to Axial Tension and Compression: A Quantum Chemical Study. *Struct. Chem.* **2015**, *26*, 11–22. DOI: 10.1007/s11224-014-0466-7.